Adsorption of Ruthenium Atoms and Clusters on Anatase TiO_2 and Tetragonal ZrO_2 (101) Surfaces: a Comparative DFT Study

Hsin-Yi Tiffany Chen, Sergio Tosoni, Gianfranco Pacchioni[1]

Dipartimento di Scienza dei Materiali,
Università di Milano-Bicocca, via Cozzi 55, 20125 Milano, Italy

Abstract

The electronic properties of a single Ru atom and a Ru_{10} cluster adsorbed on stoichiometric and reduced anatase, a-TiO_2 (101), and tetragonal zirconia, t-ZrO_2 (101) surfaces have been determined with Density Functional Theory calculations with Hubbard corrections (DFT+U). The main purpose of the work is to better understand the role of dispersed metals on the surface of titania and zirconia catalysts in conversion of biomass to biofuels. On the stoichiometric surfaces, the metal adsorption does not imply major charge transfers. The situation is different on the reduced surfaces where electron transfer occurs from the oxide to the metal; this effect is more pronounced on zirconia than on titania. On both surfaces, the presence of the Ru nanoparticle favors the removal of O from the surface layers. This can result in the occurrence of O reverse spillover, with displacement of an O atom from a lattice position of the stoichiometric surfaces to a specific adsorption site of Ru_{10}. This process is thermodynamically accessible for both TiO_2 and ZrO_2 surfaces showing that the metal deposition can result in an easier reduction of the oxide support due to this effect more than to a direct electron transfer from the metal.

Keywords

Heterogeneous Catalysis, Oxide Surfaces, Metal Nanoparticles, Quantum Chemical Calculations

[1] Corresponding author. E-mail: gianfranco.pacchioni@unimib.it (tel. +39-2-64485219)

1. Introduction

Metal clusters and nanoparticles deposited on an oxide surface are at the basis of heterogeneous catalysis, both industrial and environmental, and for this reason are intensively studied experimentally and theoretically.[1,2,3,4] The motivation of this paper is related to a specific class of catalytic reactions, i.e. the production of biofuels from cellullosic biomass.[5] A key step in this process is to lower the oxygen content and eliminate the high water content of the biomasses.[6,7,8] To achieve an industrially viable efficiency of the reaction, effective catalysts are needed. In bio-oil upgrading, metal oxides like TiO_2 and ZrO_2 are of particular interest for their activity and selectivity in the ketonization of carboxylic acids, an important step in biomass conversion.[9,10,11] Experimentally, it has been found that the ketonization rate can be enhanced by adding metal particles, such as Ru, on the surface of the oxide catalyst.[12,13] The role of the metal in enhancing the activity of the catalyst is still matter of debate. It has been suggested that the addition of Ru helps to enhance the reducibility of TiO_2 and that this should result in the easier formation of coordinatively unsaturated Ti^{3+} sites. A similar effect has been found for ZrO_2 where the activity is enhanced by the presence of Zr^{3+} ions. Another important observation, which holds true for both TiO_2 and ZrO_2, is that pre-reduction in H_2 significantly, enhances the activity of the catalyst, while the activation energies and reaction orders remain unchanged.[9] This leads to the conclusion that the pre-reduction treatment determines an increase of the active sites. While there is no doubt that reduction processes in TiO_2 and ZrO_2 may lead to an increase of Ti^{3+} and Zr^{3+} ions,[14,15] their role in the adsorption and reaction of carboxylic acids from biomass needs further studies. A possibility is that the addition of small amounts of transition metal particles like Ru favor the H_2 dissociation hence the reduction of the oxide, but other mechanisms are possible and will be discussed in this paper.

In this work we compare, using the same computational setup, the adsorption of a single Ru atom and of Ru_{10} cluster on stoichiometric and reduced anatase a-TiO_2 and tetragonal t-ZrO_2 (101) surfaces. Thermodynamically, rutile is the most stable polymorph of TiO_2 at all temperatures, exhibiting lower total free energy than the metastable phases of anatase or brookite.[16,17,18] However, anatase is the most common phase in catalytic applications.[19,20,21,22,23] ZrO_2 can exist in at least five polymorphs.[24,25] At room temperature, only monoclinic zirconia exists; at around 1480 K a transition to a tetragonal phase occurs, further converted at 2650 K into the cubic fluorite phase.[26] The most stable monoclinic polymorph has little practical applications because of the crumbling of the ceramic components commonly observed during cooling from the tetragonal phase.[27] On the contrary, the high temperature polymorphs (tetragonal and cubic) exhibit excellent mechanical, thermal, chemical and dielectric properties.[28,29] The incorporation of impurities, such as Mg or Y

cations tends to remarkably stabilize tetragonal and cubic phases, also at lower temperatures.[30,31] Here we have chosen to concentrate our attention to the tetragonal phase. However, it must be pointed out that, when focusing on surfaces, the most stable surfaces of tetragonal and cubic zirconia, (101) and (111) respectively, display exactly the same structure.[32]

We have studied the adsorption of Ru_1 and Ru_{10} on the most stable (101) surfaces of both oxides to identify the nature of the interaction of the metal with the support and to compare the behavior of the two oxides. As discussed in the computational part, the calculations have been performed at the DFT+U level in order to obtain an acceptable description of the electronic structures of the two oxides.

The paper is organized as follows. After a brief computational section (Section 2), we compare the electronic properties of a-TiO_2 and t-ZrO_2 surfaces, with particular attention to the band alignment and the stability and electronic structure of surface and sub-surface O vacancies in TiO_{2-x} and ZrO_{2-x}. Next, Section 3, we discuss the binding properties of isolated Ru atoms on the stoichiometric and reduced (101) surfaces of the two oxides. In Section 4 we describe the results for Ru_{10} adsorption on non-defective and defective TiO_2 and ZrO_2 surfaces. We also consider the possible occurrence of O spillover, i.e. migration of O atoms from the oxide surface to the metal nanoparticle with consequent reduction of the oxide. Some conclusions are reported in the last section.

2. Computational methods

All calculations are performed with the VASP 5 simulation package.[33] The core electrons are treated with the Projector Augmented Wave approach.[34,35] O(2s, 2p), Ti(3s, 4s, 3p, 3d), Zr(4s, 5s, 4p, 4d) and Ru(5s, 4p, 4d) are considered as valence electrons and treated explicitly. The exchange and correlation energy is calculated with the generalized gradient approximation (GGA) of the density functional theory, using the PBE functional.[36] To partially circumvent the well-known self-interaction error, which affects the electronic structure of semiconducting oxides calculated with GGA, we adopt the so called GGA+U approach.[37,38] This method partly removes the underestimation of the electronic band gap and the excessive tendency to delocalize the electron density.[39-41] This approach consists in defining a Hubbard's effective parameter to penalize multiple occupation for Ti and Zr d-orbitals. In the present work, we empirically set this parameter to 3 eV and 4 eV for Ti and Zr, respectively, which ensures a good qualitative description of structure and electronic properties of Ti and Zr oxides. In particular, we checked that the relaxed lattice parameters are in reasonable agreement with the experiment (i.e. errors on the cell volume are no

larger than 5-6%). Moreover, we ensured that a typical point defect such as the oxygen vacancy is properly described (see Section 3). These topics have been the subject of numerous publications in recent years.[14,42,43,44]

For the relaxation of lattice and internal coordinates of anatase TiO_2 and tetragonal ZrO_2 we used a cut-off of 600 eV and a Γ-centred high-density grid of K-points (8x8x4 for anatase TiO_2 and 8x8x8 for ZrO_2). Surface properties are studied by means of proper slab models of the most stable surfaces of a-TiO_2 and t-ZrO_2, which with our computational setup turned out to be the (101), in agreement with previous reports.[32,45,46,47,48] Convergence of the surface energy is reached for five-MO_2 layer models (M = Ti or Zr).

Deposition of a single Ru atom is simulated on 2x1 supercells of a-TiO_2 and t-ZrO_2 (101) surfaces. Ru_{10} metal clusters are studied in larger supercells, 3x1 and 3x2 for TiO_2 and ZrO_2, respectively. In all cases, at least 10 Å of empty space above the adsorbate is included to avoid spurious interactions between the replicas of the slab model.

For all models, we perform structural relaxations of all atoms with convergence criteria of 10^{-5} eV and 10^{-2} eV/Å for the electronic and ionic loops, respectively. The sampling of the reciprocal space is reduced to a 2,2,1 mesh for the 2x1 supercell of ZrO_2 and to the Γ-point only for the other cases. This choice is justified by the large dimension of the supercells. Atomic charges are computed using the decomposition scheme proposed by Bader.[49]

3. Results and discussion

3.1 Stoichiometric and reduced a-TiO_2 and t-ZrO_2 surfaces

The (101) surface of a-TiO_2 displays 2- and 3-coordinated oxygen atoms (O_{2c} and O_{3c}, respectively), while the (101) surface of t-ZrO_2 exhibits only O_{3c} sites. Both surfaces are remarkably stiff, i.e. the surface ions display a limited relaxation compared to the bulk lattice positions. We adopt stoichiometric oxygen-terminated models for both oxides.

3.1.1 Stoichiometric a-TiO_2 and t-ZrO_2

In Figure 1 we report the density of states (DOS) curves of a-TiO_2 and t-ZrO_2 (101) surfaces. With the adopted computational setup, the TiO_2 surface displays a band gap of 2.6 eV. The bulk value, 2.4 eV, is underestimated with respect to the experiment, 3.2 eV.[22] The fact that the gap is smaller in the bulk than on the surface is due to the problem of oscillations of the band gap in titania with the number of layers.[50] A correct reproduction of the band gap would require very high values of the U parameter in DFT+U, a choice that can severely affect other properties and in particular the surface

reactivity.[51] Also the band gap of the t-ZrO_2 (101) surface (3.8 eV) is smaller than that calculated for the bulk (4.5 eV), as should be expected due to the presence of surface atoms with lower coordination. Also for ZrO_2 the bulk value, 4.5 eV, is underestimated with respect to experiment for the same reasons mentioned above (there are several values reported in the literature for the band gap of ZrO_2; recent estimates give an approximate value of about 5.0 eV;[15] Electron energy loss spectroscopy (EELS) gives 4.2 eV [52] while Vacuum ultraviolet absorption spectroscopy measurements give values between 5.8 and 6.6 eV[53]).

The projected DOS, pDOS, Figure 1, reveal that, for both oxides, the valence band (VB) is mainly due to O 2p orbitals, while Ti 3d or Zr 4d orbitals prevail in the composition of the conduction band (CB). The alignment of the energy levels with respect to vacuum, Figure 1, allows us to directly compare the position of the bands of the two surfaces. This is an important information to rationalize the behaviour of supported metal particles on these two oxides. The edges of both occupied and virtual states of TiO_2 lie at lower energy compared to those of ZrO_2, indicating that TiO_2 is more reducible than ZrO_2. In particular, the top of the VB in a-TiO_2 is calculated at -7.3 eV. A recent study of band alignment in anatase TiO_2 based on combined hybrid functional calculations and XPS measurements places the value of the top of the VB at -8.3 eV, i.e. about 1 eV lower than in our case.[54] On the contrary, the position of the bottom of the CB, -4.7 eV, Figure 1, is close to the estimate of ref. 54, -5.1 eV. The too high value of the top of the VB is also the main reason for the too small band gap in a-TiO_2(101) surface with the present computational approach. In t-ZrO_2 the top of VB is found at -6.6 eV and the bottom of the CB at -2.8 eV, with a band gap of 3.8 eV. A direct comparison with experiments in this case is complicated by the scattered values of the band edges as a function of the method used. These results are consistent with TiO_2 being easier to reduce (lower CB minimum) and harder to oxidize (lower VB maximum) than ZrO_2.

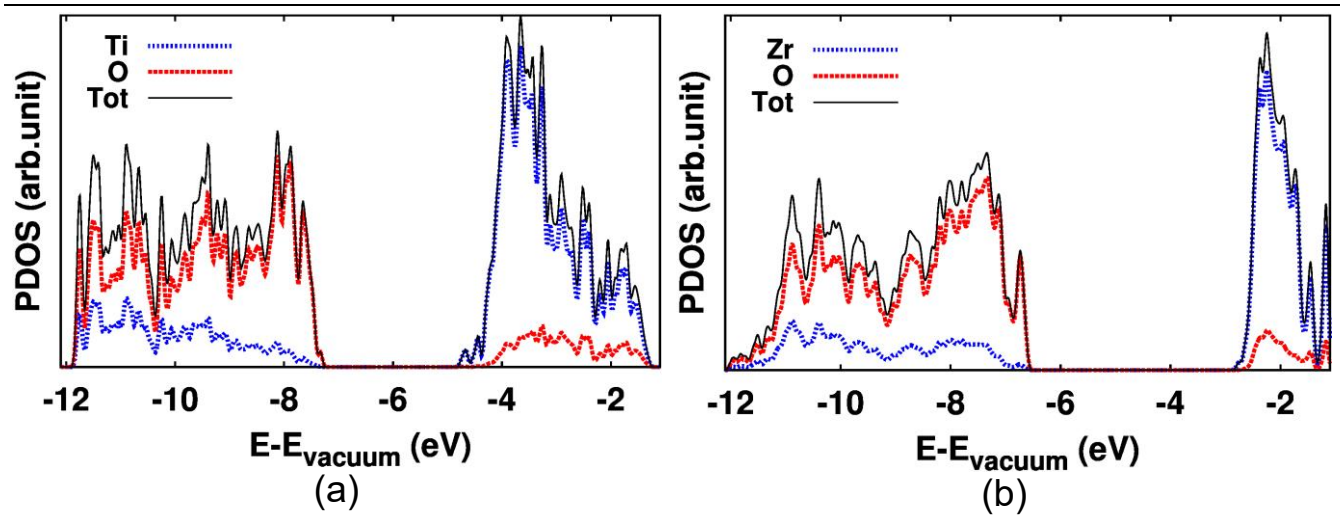

Figure 1. Total and projected density of states of (101) surfaces of (a) a-TiO_2 and (b) t-ZrO_2. Energies with respect to the vacuum level set to zero.

3.1.2 Reduced a-TiO_{2-x} and t-ZrO_{2-x}

The electronic structure of reduced anatase TiO_{2-x} has been the subject of many theoretical studies and does not need to be discussed.[14] Also reduced ZrO_2 has been addressed previously,[15] although the number of studies on this system is smaller than on TiO_2. Here we discuss only those elements that are essential for the comparison of the two systems and for the analysis of the metal/oxide interaction. We model reduced TiO_{2-x} and ZrO_{2-x} (101) surfaces by creating an oxygen vacancy (V_O) in various positions like surface, sub-surface and bulk sites, Figure 2.

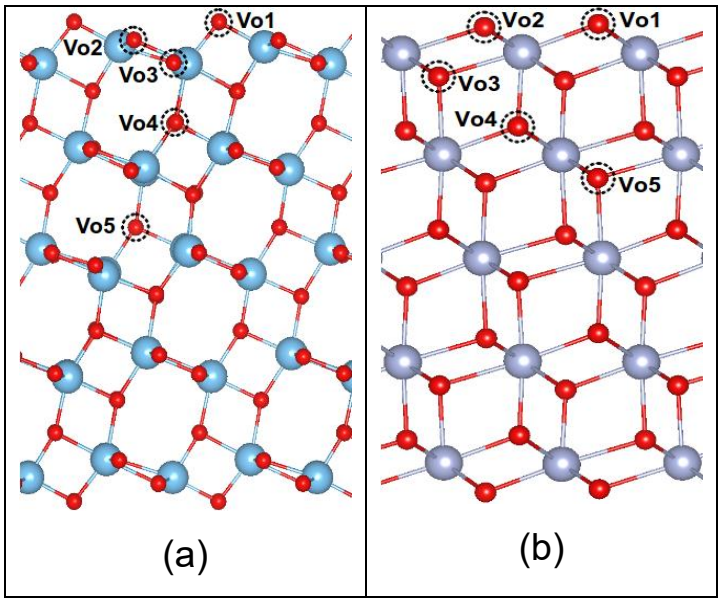

Figure 2. Side view of oxygen vacancy sites, V_O, in (101) slabs of (a) a-TiO_2 and (b) t-ZrO_2. See also Table 1. Red: O; blue: Ti; violet: Zr.

The reducibility of the oxide surface is determined by the formation energy of an O vacancy with respect to the stoichiometric oxide and a gas-phase oxygen molecule:

$$\Delta E_{vac} = E(MO_{2-x}) - E(MO_2) + \tfrac{1}{2}\, E(O_2) \qquad (M = Ti, Zr) \qquad (1)$$

In Table 1, we report ΔE_{vac} and the total number of unpaired electrons ($N_\alpha - N_\beta$) for various V_O centers in a-TiO_2 and t-ZrO_2 (101) surfaces. The anatase (101) surface displays non-equivalent

surface oxygen atoms, O_{2c} and O_{3c} sites. O_{3c} sites can be further distinguished according to the nature of the closest Ti ions, Ti_{5c} or Ti_{6c}. This variety of sites reflects in rather different stabilities of the vacancies. The removal of an O_{2c} atom leads to the most stable structure with ΔE_{vac} = 4.53 eV (V_O1). The removal of an O_{3c} has an higher cost, 5.82 eV (Ti_{6c} case, V_O2) or 5.35 eV (Ti_{5c}, V_O3). When moving away from the surface, toward the sub-surface layer and the bulk zone, the formation energy decreases to 4.78 eV (sub-surface V_O4) and 4.72 eV (bulk V_O5). The lowest configuration is always magnetic, with two unpaired electrons localized on two Ti^{3+} ions. However, singlet open shell solutions are very close in energy and result from spin contamination. A detailed analysis of the magnetic nature of the ground state is however outside the scope of this work.

The finding that it is easier to remove an O atom from the surface than from the deeper layers contrasts with the results reported by Selloni et al.[55,56,57] on this topic. This discrepancy, which reflects the very similar formation energies of O vacancies in different positions, is due to the slightly different computational setup used, like for instance the choice of the U parameter in DFT+U.

Table 1. Formation energy, ΔE_{vac}, and number of unpaired electrons, $N_\alpha - N_\beta$, of oxygen vacancies in a-TiO_2 and t-ZrO_2 (101) surfaces

			ΔE_{vac}, eV	$N_\alpha - N_\beta$
a-TiO_2	Surface	V_O1, O_{2c}	4.53	2
	Surface	V_O2	5.82	2
	Surface	V_O3	5.35	2
	Sub-surface	V_O4	4.78	2
	Bulk	V_O5	4.72	2
t-ZrO_2	Surface	V_O1	6.04	2
	Surface	V_O2	5.89	0
	Sub-surface	V_O3	5.49	0
	Subsurface	V_O4	5.58	0
	Bulk	V_O5	5.55	0

For ZrO_2, two possible surface vacancies are found: one with a triplet ground state and a formation energy of 6.04 eV, V_O1, and the other one with singlet closed shell configuration and ΔE_{vac} = 5.89 eV (V_O2). The most stable vacancy is V_O3, obtained by removing an oxygen from sub-surface; the formation energy is 5.49 eV. By further moving towards the bulk region, we encounter

structures of comparable stability, 5.58 eV (V_O4) and 5.55 eV (V_O5). All oxygen vacancies in subsurface and bulk regions lead to singlet structures.

From these data we can conclude that energetically the formation of a vacancy on anatase TiO_2 costs about 1 eV less than on ZrO_2, in agreement with the general view of titania being easier to reduce than zirconia.

In Figure 3 we report the pDOS curves for surface and sub-surface V_O defects in a-TiO_2 and t-ZrO_2. The presence of the vacancy induces occupied states in the gap due to the formation of reduced Ti- or Zr-centers. The precise location of the defect states in the gap depends on the position of the vacancy (shallower for surface vacancies, deeper for sub-surface ones) and on the nature of the oxide (in TiO_2 the gap states are more shallow than in ZrO_2). In a-TiO_2 the defect states corresponding to Ti^{3+} ions are at about 0.3-0.7 eV below the bottom of the CB, Figure 3a. This is close to experimental measurements that indicate the formation of defect states just below the bottom of the CB. In bulk or sub-surface sites of ZrO_2 the creation of an O vacancy leads to a doubly occupied state about 2.3-2.6 eV, depending on the site, above the top of the VB, Figure 3d. The two trapped electrons are shared among the four Zr ions around the vacancy. This is consistent with recent results on the V_O center in the bulk of tetragonal zirconia obtained with the hybrid B3LYP functional;[15] in this work the defect state is found at about 3.3 eV above the VB but the band gap is 5.8 eV, compared to a gap of 4.5 eV obtained here using the DFT+U approach. The fact that the extra electrons are largely localized in the cavity left by the removed O atom is common to both DFT+U and B3LYP treatments. In this respect, the bulk O vacancy in ZrO_2 closely resembles a neutral F center in alkaline-earth oxides. Things are different on the surface where the ground state of the defect is magnetic, Figure 3c, with two unpaired electrons localized on surface Zr^{3+} ions close to the defect.

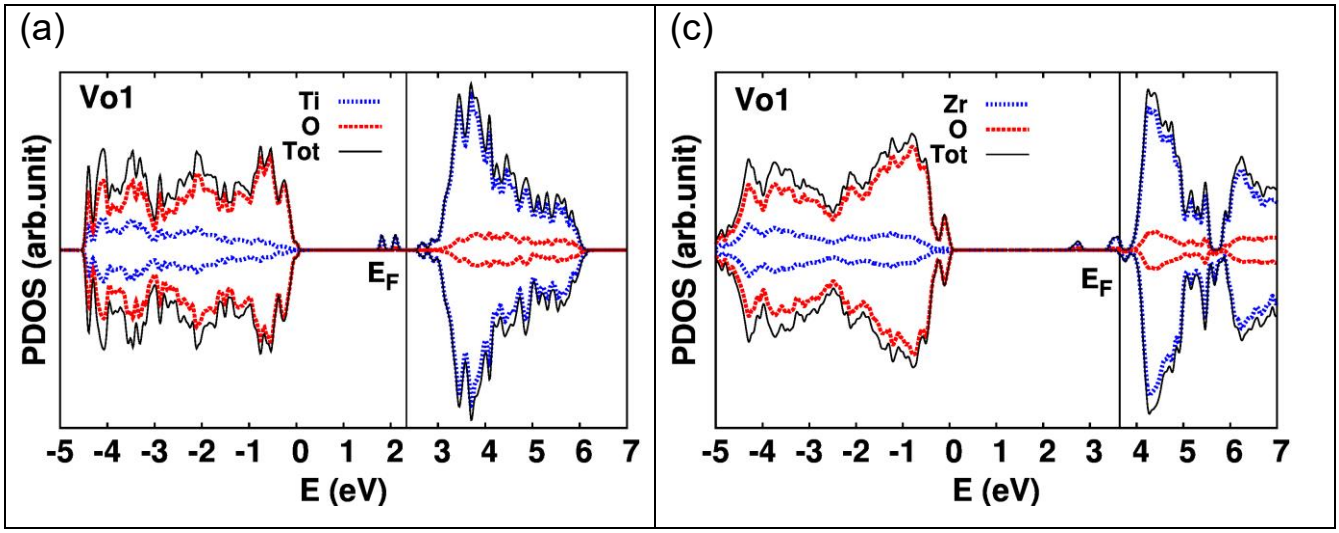

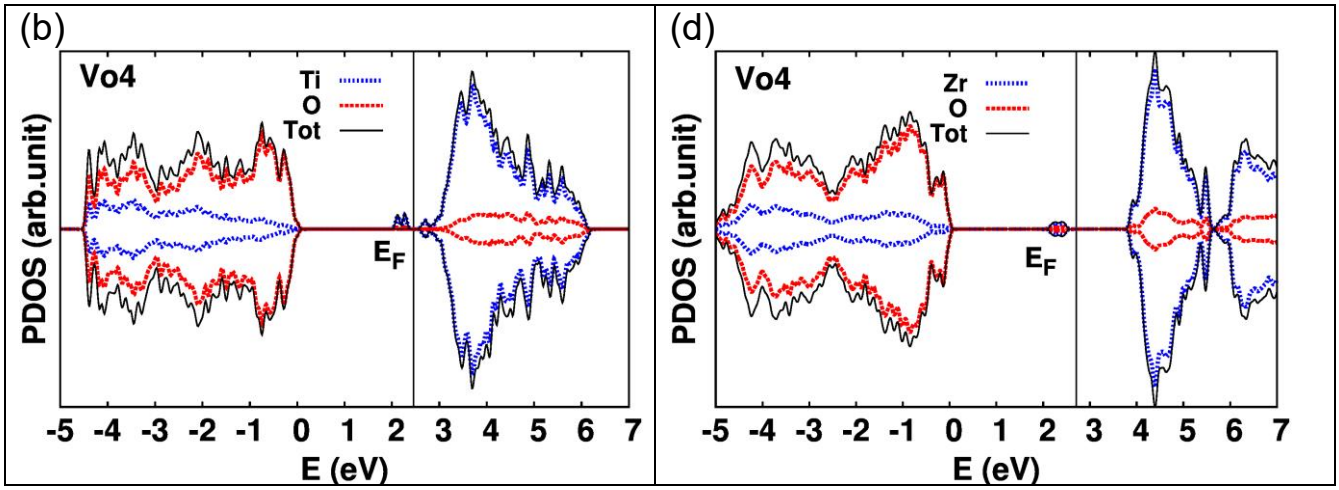

Figure 3. Left: Density of states of oxygen vacancies in a-TiO_2(101); (a) surface, V_O1; (b) sub-surface, V_O4. Right: Density of states of oxygen vacancies in t-ZrO_2(101); (c) surface, V_O1; (d) sub-surface, V_O4. The zero of energy corresponds to the maximum of the valence band.

3.2 Ru atom adsorption on a-TiO_2 and t-ZrO_2

Until a few years ago the study of isolated metal atoms on a support for catalytic purposes was mostly restricted to theoretical calculations dealing with the general problem of supported metal nanoparticles. In the last years, however, also thanks to the use of more sophisticated techniques like transmission electron microscopy with aberration correction, the existence of single atom catalysts has been proven and these systems have gained more attention due to their potential role in catalytic reactions.[58,59,60,61] Here we consider the properties of single Ru atoms adsorbed on stoichiometric and reduced a-TiO_2 (101) and t-ZrO_2 (101) surfaces.

3.2.1 Ru_1 on stoichiometric a-TiO_2 and t-ZrO_2

Various possible adsorption sites of a Ru adatom have been considered. It turns out that the preferred adsorption sites are quite different for the two surfaces. On a-TiO_2 the adsorption occurs preferentially on a hollow site where Ru is coordinated to four O atoms, two O_{2c} and two O_{3c}; the metal atom is almost incorporated into the hollow site and lies in the same plane of the O atoms of the oxide support, Figure 4(a). On t-ZrO_2 the most stable site is in a bridge position between two O_{3c} atoms, and the Ru atom protrudes above the surface and thus is much more exposed than on TiO_2, Figure 4(d).

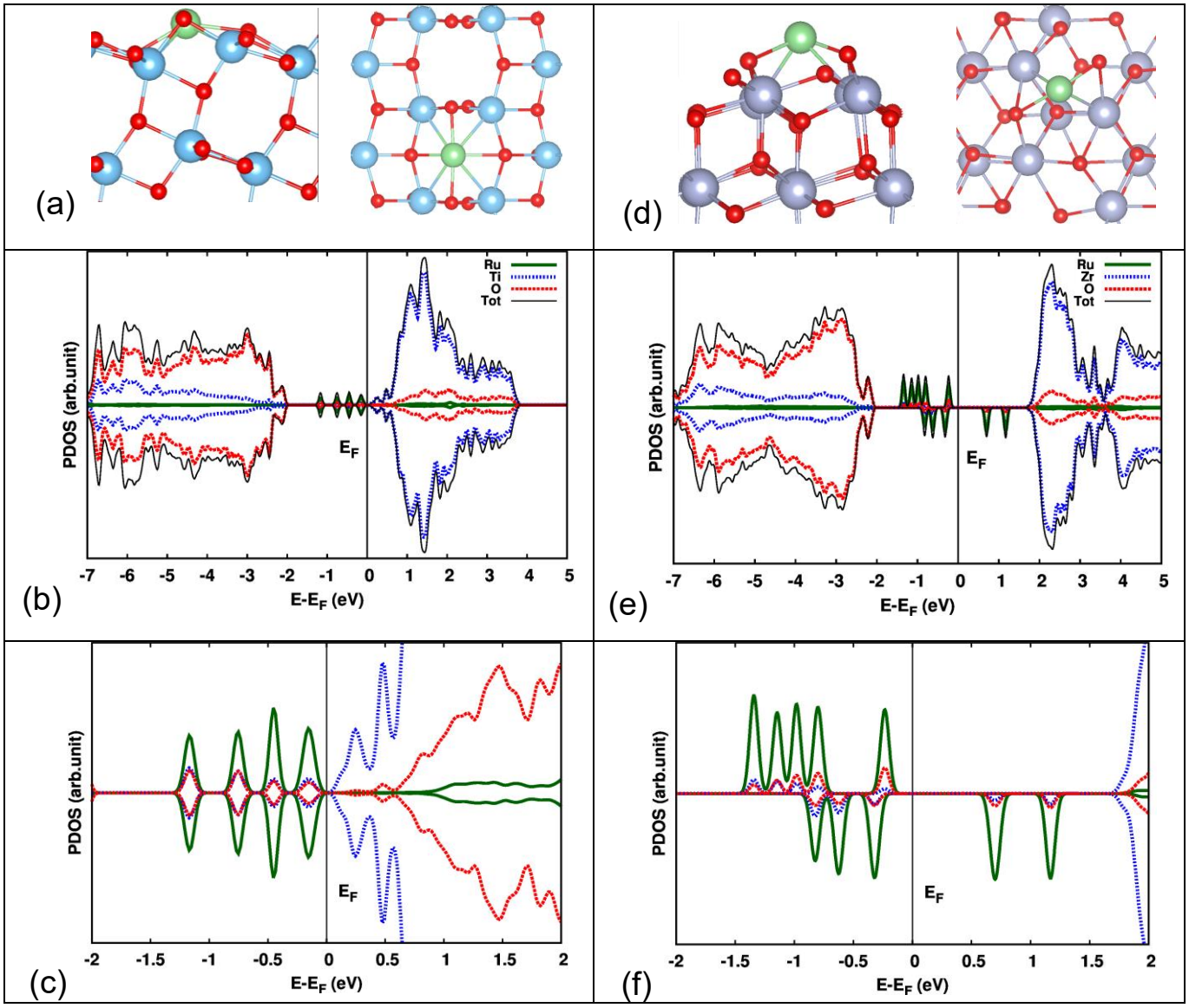

Figure 4. Left: Ru atom adsorption on a-TiO_2(101); (a) Structures (side and top view); (b) projected DOS; (c) 3d region. Right: Ru atom adsorption on t-ZrO_2(101); (d) Structures (side and top view); (e) projected DOS; (f) 4d region. The zero of energy corresponds to the Fermi level.

In Table 2 we report the adsorption energy of Ru on the two oxide surfaces (E_{ads}), the total magnetic moment, and the Bader charge. E_{ads} is defined as:

$$E_{ads} = E(Ru_n/MO_{2-x}) - E(MO_{2-x}) - E(Ru_n, \text{gas phase}) \qquad (M=Ti, Zr;\ n = 1, 10) \qquad (2)$$

For Ru on a hollow site of a-TiO_2 E_{ads} is -2.99 eV. The Ru-O_{2c} bond lengths are 2.04 Å while different Ru-O_{3c} bond lengths of 2.06 and 2.20 Å, respectively, are found. This is consistent with

the results found by Zhang et al. on the same system.[62] The adsorption mode is characterized by a covalent-polar bond with partial depletion of the electronic charge from Ru which, according to the Bader analysis, has a charge q = +0.6 |e|, Table 2. However, formation of Ti^{3+} ions is not observed as shown by both the pDOS curves, Figure 4(b) and (c), and the spin density plots, Figure 5(a). The formation of Ti^{3+} ions would be indicative of the occurrence of a net charge transfer, and should also result in a change in configuration of the Ru atom. On a-TiO_2 Ru has a $4d^8$ configuration, Figure 4(c), i.e. the same number of valence electrons of the free atom ($4d^7\ 5s^1$). The change in configuration from $4d^7\ 5s^1$ to $4d^8$ is a consequence of the interaction with the surface and is also at the origin of the complete quenching of the magnetic moment from quintet (free atom) to singlet (supported atom). We have also considered a solution where the system is forced to have two unpaired electrons (triplet) to check other possible configurations for the Ru atom. The results, Table 2 and Figure S1, clearly show that one unpaired electron is on Ru and the other one is delocalized over several Ti ions. This means that a charge transfer has occurred; the Ru atom has assumed a $4d^7$ configuration with consequent reduction of the TiO_2 surface, Table 2. Attempts to localize the transferred electron failed. This charge transfer solution is slightly higher in energy than the previous one (by 0.17 eV), Table 2.

Table 2. Adsorption energy, E_{ads}, number of unpaired electrons, N_α–N_β, and Bader charge, q, of Ru atom adsorbed on stoichiometric and reduced a-TiO_2 and t-ZrO_2 (101) surfaces

	Surface	Supercell	Adsorption site	E_{ads} (eV)	N_α–N_β		Ru Config.	q(Ru) |e|
					Ru	MO_2		
a-TiO_2	Stoichiometric	$Ti_{40}O_{80}$	Hollow	-2.99	0.0	0.0	$4d^8$	+0.61
	Stoichiometric	$Ti_{40}O_{80}$	Hollow	-2.82	0.9	0.8	$4d^7$	+0.82
	Reduced	$Ti_{40}O_{79}$ (V_O1)	V_O top	-3.22	0.0	0.0	$4d^{10}$	-0.18
	Reduced	$Ti_{40}O_{79}$ (V_O4)	Hollow	-2.53	0.0	+0.8,-0.7	$4d^8$	+0.51
t-ZrO_2	Stoichiometric	$Zr_{20}O_{40}$	Bridge	-2.45	1.7	0.1	$4d^8$	+0.18
	Reduced	$Zr_{20}O_{39}$ (V_O1)	V_O top	-3.99	1.9	-0.1	$4d^8$	-0.80
	Reduced	$Zr_{20}O_{39}$ (V_O4)	Bridge	-2.65	1.0	0.5	$4d^9$	-0.19

On the bridge site of stoichiometric t-ZrO_2 Ru is bound with E_{ads} = -2.45 eV. The Ru atom lies 2.1 and 2.7 Å away from the closest O and Zr ions, respectively. The ground state configuration is $4d^8$, Figure 4(e) and (f), and shows the presence of two unpaired electrons, Figure 5(d), with a

partial quenching of the magnetic moment of the free Ru atom. According to the Bader charge, on t-ZrO_2 the Ru atom almost preserves its neutrality; the small positive charge of +0.18 |e| originates from a mixing of the Ru and O 2p orbitals and indicates only a moderate charge displacement. As reported in the case of TiO_2, formation of Zr^{3+} ions is not observed, excluding a direct reduction of the support, Figure 5(d). For comparison, coinage metals (Cu, Ag, Au) are adsorbed preferentially on O-Zr bridge sites of the (111) surface of cubic ZrO_2 with a weaker adsorption energy (smaller than 1 eV).[63]

The metal ad-atom introduces a manifold of occupied and empty states in the oxide band gap, Figure 4(c) and (f). In the case of a-TiO_2 these states are closer to the conduction band.

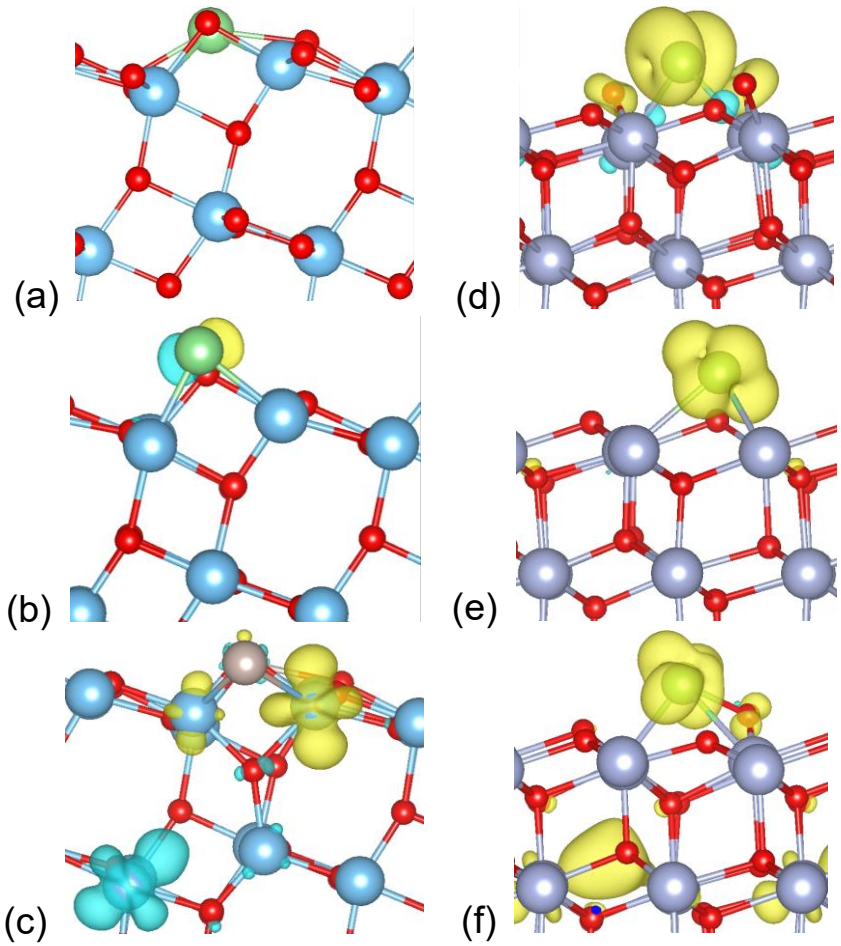

Figure 5. Left: spin density plots of Ru adsorbed on a-TiO_2; (a) $Ti_{40}O_{80}$; (b) $Ti_{40}O_{79}$ (V_O1); (c) $Ti_{40}O_{79}$ (V_O4). Right: spin density plots of Ru adsorbed on t-ZrO_2; (d) $Zr_{20}O_{40}$; (e) $Zr_{20}O_{39}$ (V_O1); (f) $Zr_{20}O_{39}$ (V_O4).

On the basis of these results we can conclude that the adsorption of Ru on the two oxide

surfaces has similar strength, about 3 eV on TiO_2 and about 2.5 eV on ZrO_2, but that the different morphology of the two surface leads to quite different bonding modes. In the case of titania the presence of open hollow sites leads to a stronger bond, a more pronounced polarization of the electronic charge towards the oxide, and the incorporation of Ru into the surface layer. On the (101) surface of t-ZrO_2 the Ru atom is almost charge neutral and protrudes from the surface. On this basis, quite different reactivity is expected for isolated Ru atoms on the two oxide supports. However, in neither TiO_2 nor in ZrO_2 we find evidence of a direct reduction of the oxide by simple deposition of the Ru atoms.

3.2.2 Ru_1 on reduced a-TiO_{2-x} and t-ZrO_{2-x}

Now we consider Ru adsorption on the reduced surface. This may take place directly on top of a surface vacancy, V_O1, or in the same sites described for the stoichiometric samples with the vacancy located in a sub-surface site. The adsorption of Ru on top of a V_O1 site, Figure 6(a) and 6(d), is always stronger than on the non-defective surface (-3.22 eV versus -2.99 eV on TiO_2, and -3.99 eV versus -2.45 eV on ZrO_2, Table 2). Thus, while on TiO_2 the increase of stability is modest; on ZrO_2 the effect is very pronounced. This can be quite relevant in terms of reducing the mobility of the surface species and their tendency to aggregate and sinter, a serious drawback in heterogeneous catalysis. Atom diffusion on the surface depends on the diffusion barrier. When different adsorption sites have very similar adsorption energies, like on regular and defect sites of a-TiO_2, Table 2, the barrier is also expected to be relatively low and diffusion to occur already at low temperatures. When defective and regular adsorption sites have very different adsorption energies, like on t-ZrO_2, the barrier is also going to be significant. In fact, the minimum energy to move a Ru atom from a V_O site to a regular site in t-ZrO_2 is of about 1.5 eV, Table 2, and the actual barrier will be even larger. This suggests that in the presence of O vacancies on the t-ZrO_2 (101) surface isolated atoms can be stabilized and their mobility can be strongly reduced. This effect is much less pronounced on a-TiO_2.

We consider now the electronic structure. Remember that on both TiO_2 and ZrO_2 a surface vacancy has two unpaired electrons localized on Ti or Zr ions, Table 1 and Figure 3. The value of the Bader charge on Ru, Table 2, suggests the occurrence of a charge transfer from the reduced oxide to the Ru atom. However, while on reduced TiO_2 this electron transfer is only partial, -0.18 |e|, on ZrO_2 it is substantial, -0.8 |e|. Net charges are not physical observables and they are obtained from a more or less rigorous partitioning of the charge density among atoms. More relevant for the discussion is the analysis of the spin density. On a-TiO_2 there is no residual spin density on Ru nor

on the vacancy after adsorption, Table 2 and Figure 5(b). This means that a spin pairing occurs between the two electrons in the defect site and the 4d electrons of Ru, with formation of a covalent bond. This is clearly shown by the pDOS curves, Figure 6(b) and (c): there are five doubly occupied 4d states in the gap, corresponding to a formal configuration $4d^{10}$ for Ru, which explains the absence of magnetization. Notice that this corresponds to a formal charge on Ru of -2, in clear contradiction with the Bader charge of -0.18 |e|, Table 2.

On t-ZrO_2, the spin on Ru is the same as for the stoichiometric surface, triplet, while no spin density is left on the surface, Table 2. In the presence of a net charge transfer, as suggested by the Bader charge of -0.8 |e|, the configuration of Ru should become $4d^9$ with a single unpaired electron. On the contrary, Ru is still $4d^8$, as indicated by the pDOS, Figure 6(e) and (f), and by the spin population, Figure 5(e), showing the presence of two unpaired electrons. We conclude that the value of the Bader charge is misleading, and that while the electrons of the vacancy are partially delocalized over the Ru atom via covalent bonding, the formal configuration of Ru remains unchanged, $4d^8$, compared to the regular surface.

We consider now the case where Ru atom adsorbs on a reduced oxide where the O vacancy is in deeper layers, not on the surface. On a-TiO_{2-x} with a sub-surface vacancy E_{ads} = -2.53 eV is smaller (in absolute value) than on the stoichiometric surface (-2.99 eV); on t-ZrO_2 with sub-surface V_O E_{ads} = -2.65 eV is similar to the stoichiometric case (-2.45 eV), Table 2. The similarity of the binding energies could suggest a similar bonding mechanism on the two oxides. However, this is not the case. For a-TiO_2 there is clear evidence that the two extra electrons associated to the vacancy are still located on two Ti^{3+} atoms (see Figure 5(c), Table 2 and Figure S2 (c)) and are not transferred to the Ru adatom. The charge on Ru is similar to that of the stoichiometric case. The sub-surface vacancy is not affected by the presence of Ru, and the bonding is similar to the non-defective surface. Therefore, on a-TiO_2 only when the O vacancy and the Ru atom are in direct contact a stronger interaction and a partial charge transfer occur.

On ZrO_2 the presence of a sub-surface vacancy has a completely different effect. The V_O center in the bulk of ZrO_2 has a singlet configuration with two electrons trapped in the vacancy, Figure 3. When a Ru atom is adsorbed on this system, a spin density appears in the cavity due to the formation of a V_O^+ center , Figure 5(f), and the number of unpaired electrons on Ru is reduced from two to one, Table 2. This is consistent with a Ru $4d^9$ configuration indicating that one electron is transferred from the vacancy (from V_O to V_O^+) to the Ru atom (from $4d^8$ to $4d^9$). Also in this case the Bader charge is not able to grasp the essence of this bonding mechanism as only a small negative charge of -0.19 |e| is found on Ru, due to the hybridization of the Ru 4d and O 2p orbitals.

However, the occurrence of an electron transfer is clear from the pDOS, Figure S2(f), and the spin density plots, Figure 5(f). The fact that this phenomenon occurs on ZrO_2 and not on TiO_2 is related to the different position of the defect states in the gap of the two oxides, Figure 3.

Ru adsorption on a reduced oxide with sub-surface or bulk vacancies shows also another interesting phenomenon. On reduced ZrO_{2-x}, in particular when the O vacancy is sub-surface (V_O3, see Figure 2), we observe a strong reconstruction. A surface O atom moves towards the sub-surface vacancy, leaving behind a vacancy in V_O1 position, in direct contact with Ru. This process is spontaneous, indicating that migration of O vacancies from bulk or sub-surface towards the surface can be simply induced by Ru atoms deposition. The process can be favoured by a mild thermal annealing but, at least for sub-surface vacancies, is non activated. The same trend is found also for TiO_2 since Ru adsorption on a surface O vacancy is preferred compared to the case where the vacancy lies sub-surface, Table 2. However, in this case we have no evidence of a spontaneous migration of a vacancy from the internal layers to the surface of a-TiO_2, indicating an activated process.

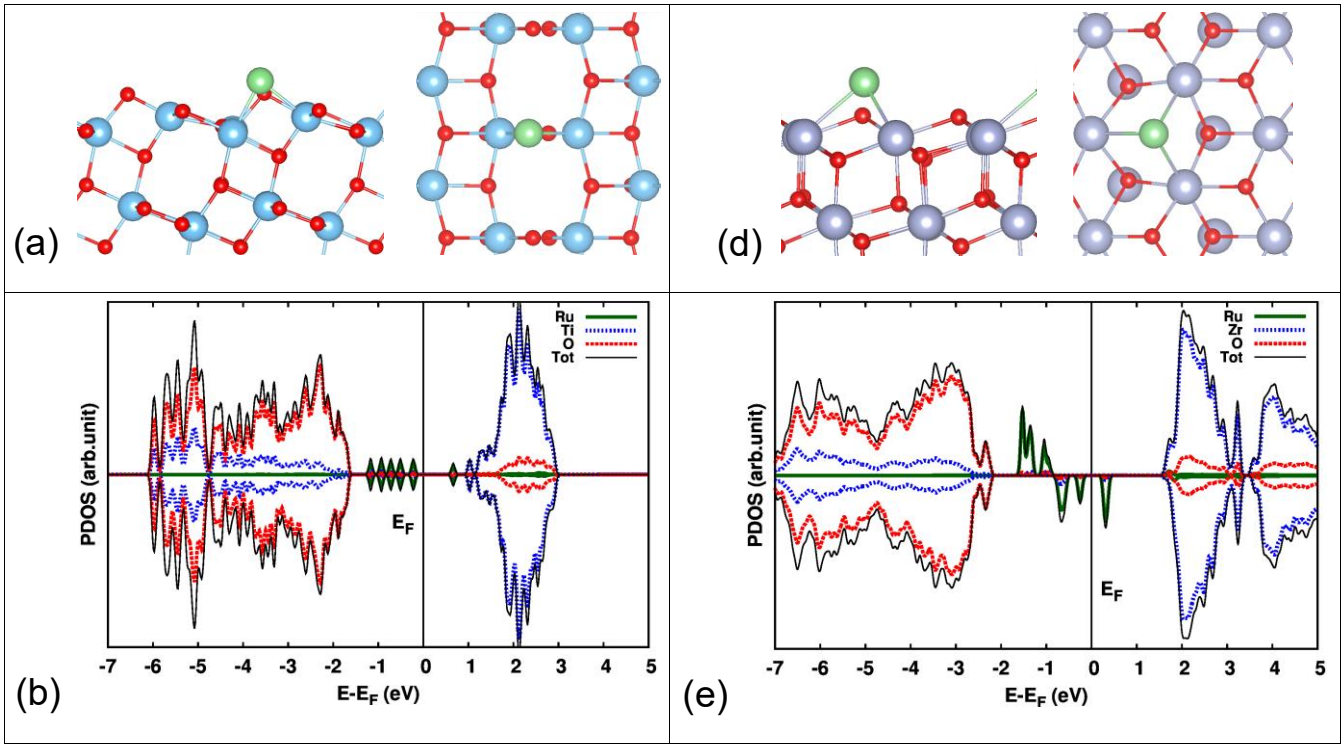

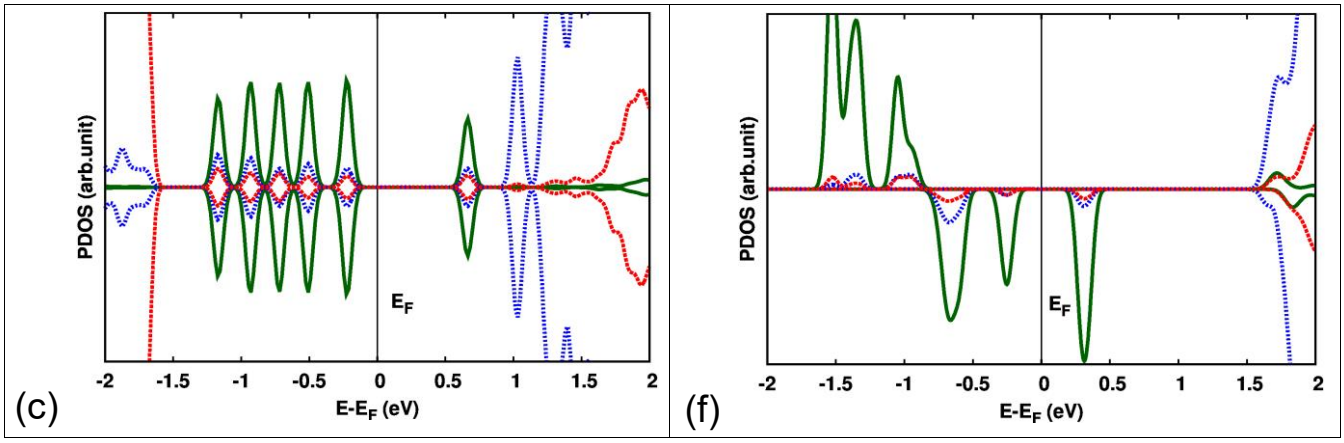

Figure 6. Left: Ru atom adsorption on a-TiO_{2-x}(101); (a) Structures (side and top view); (b) projected DOS; (c) 3d region. Right: Ru atom adsorption on t-ZrO_{2-x} (101); (d) Structures (side and top view); (e) projected DOS; (f) 4d region. The zero of energy corresponds to the Fermi level.

3.3 Ru_{10} adsorption on a-TiO_2 and t-ZrO_2

The theoretical study of metal clusters on a supporting oxide surface is complicated by the existence of several minima. A gas-phase 10-atoms cluster has a large number of possible isomers, often separated by tiny energy differences. The situation can be even more complex on a surface. The search for the global minimum is not only computationally very intensive and requires specific methods like molecular dynamics with simulated annealing or the use of genetic algorithms,[64] but it is also delicate in terms of outcome, as different computational methods can provide rather different structures. This is not surprising if we consider the fluxional nature of metal clusters and the easy interconversion of an isomer into another one. In particular, when there is sufficient thermal energy at disposal, a cluster on a surface is not a rigid object but rather a kind of liquid nano-droplet that can continuously change shape and structure. Here we are interested in the chemical and electronic modifications that are induced by the formation of small aggregates of Ru atoms on the surface of titania and zirconia. The search for a global minimum is outside the scope of the present work. Rather, we are interested in understanding the mutual interaction of each oxide with a Ru nanoparticle. To this end we use a Ru_{10} two-layer cluster as a model of Ru nanoparticles. The Ru_{10}(7,3) cluster is a hemi-spherical section of a Ru_{13} cluster with cubo-octahedral shape with seven atoms in the bottom plane and three atoms in the upper plane. This structure is useful to model a supported cluster since it has a large metal-oxide interface, which favours the adhesion of the cluster to the support, and a second layer of metal atoms which are exposed to the vacuum region

and are only indirectly affected by the presence of the oxide support. Starting from this configuration, the Ru_{10}(7,3) cluster has been optimized both in the gas-phase and on the a-TiO_2 (101) and t-ZrO_2 (101) supports. Several starting points have been considered for the geometry optimization, so that a partial exploration of the complex potential energy surface has been performed. Still, we cannot exclude that more stable isomers exist. From this search a number of structures have been obtained, some of which retain the original (7,3) structure. They will be discussed first since they allow to separate the electronic effects due to the cluster-surface interaction from other effects related to the more or less pronounced rearrangement of the atoms in the cluster (these have been observed only for the anatase TiO_2 surface).

3.3.1 Ru_{10} on stoichiometric a-TiO_2 and t-ZrO_2

We start considering Ru_{10} on a-TiO_2. The central Ru atom of the bottom layer has been placed on top of an O_{2c} or an O_{3c} atom of the surface. The O_{3c} site appears to be more strongly binding (E_{ads} = -5.99 eV on O_{3c} compared to E_{ads} = -4.70 eV on O_{2c}). The reason for the different stability is that there are only three Ru-O_{2c} bonds in the first structure, Figure 7(a), and four in the second one. Since O_{2c} sites are more reactive, this can provide a general principle for the adhesion of Ru particles to anatase. For the most stable geometry, the Ru-O and Ru-Ti bond lengths are around 2.1 and 2.7 Å, respectively.

The Bader charge of the Ru_{10} cluster is 1.18 |e|, suggesting the occurrence of an electron transfer from Ru_{10} to the TiO_2 surface, which is consistent with previous work.[62,65] As we have seen above, Bader charges must be taken with some care. Still, to gain further insight, we have decomposed the charge on the cluster into individual atomic contributions and found that the Ru atoms bound to surface O atoms have charges of +0.2 |e| or more; the Ru atoms bound to both O and Ti atoms have charges between +0.05 and +0.26 |e|, while the Ru atoms not in contact with the TiO_2 surface or bound only to Ti sites are slightly negative, -0.02 ~ -0.14 |e|. However, no evidence of the formation of Ti^{3+} ions is found even after artificial distortion of the lattice to favor the formation of the small polaron around the Ti^{3+} center. This clearly indicates that the Ru_{10} cluster is bound to TiO_2 mainly *via* Ru-O covalent bonds and that there is a moderate electron polarization from Ru to O which without occurrence of a direct charge transfer. Ru_{10} does not induce a reduction of the oxide surface. We also notice that there are nearly four unpaired electrons on Ru_{10}, two with spin up and two with spin down, Table 3, indicating an antiferromagnetic ordering that is probably due to spin contamination effects.

Table 3. Adsorption energy, E_{ads}, number of unpaired electrons, N_α–N_β, and Bader charge, q, of Ru_{10} adsorbed on stoichiometric and reduced a-TiO_2 and t-ZrO_2 (101) surfaces.

	Surface	Supercell	Adsorption site	E_{ads} (eV)	N_α–N_β		q (Ru_{10})
					Ru_{10}	MO_2	|e|
a-TiO_2	Stoichiometric	$Ti_{60}O_{120}/Ru_{10}$(7,3)	O_{3c}	-5.99	+1.9,-1.9	-0.1	+1.18
	Stoichiometric	$Ti_{60}O_{120}/Ru_{10}$(6,4)	-	-6.94	2.8	0.3	+1.28
	Reduced	$Ti_{60}O_{119}/Ru_{10}$	V_O1	-8.20	+2.5,-0.9	0.2	+0.50
	Reduced	$Ti_{60}O_{119}/Ru_{10}$	V_O4	-5.95	1.5,-1.5	1.3	+1.02
t-ZrO_2	Stoichiometric	$Zr_{60}O_{120}/Ru_{10}$	O_{3c}	-8.49	+1.9,-0.1	0.0	+0.28
	Reduced	$Zr_{60}O_{119}/Ru_{10}$	V_O1	-10.73	+0.5,-0.5	0.0	-0.49
	Reduced	$Zr_{60}O_{119}/Ru_{10}$	V_O4	-8.40	+1.9,-0.1	0.0	+0.26

A similar procedure has been followed for Ru_{10} on t-ZrO_2. The central Ru atom in the bottom layer of Ru_{10} has been placed on top of O or on-top of Zr, with the former clearly more stable. The adsorption energy of Ru_{10} on-top of O, -8.49 eV, is considerably higher than that of the corresponding isomer on a-TiO_2 (-5.99 eV), Table 3. Differently from the anatase surface, a major structural rearrangement occurs on the ZrO_2 surface upon deposition of Ru_{10}. In fact, the O_{3c} atom just below the cluster moves down significantly to allow a closer interaction between the cluster and the surface, Figure 7(c). The final Ru-O and Ru-Zr bond lengths, about 2.0 and 2.8 Å, are not very different from those found on TiO_2. The local atomic rearrangement of the zirconia surface leads to an almost undistorted Ru_{10} cluster, Figure 7(c). In other words, the strain at the metal/oxide surface is distributed on the oxide more than on the metal. The Bader charge on the entire cluster is 0.28 |e|, and there is no evidence of the formation of Zr^{3+} ions indicating that practically there is no direct reduction of the oxide surface by deposition of Ru_{10} (even attempts to localize the charge on Zr by distorting the structure did not result in the formation of Zr^{3+}).

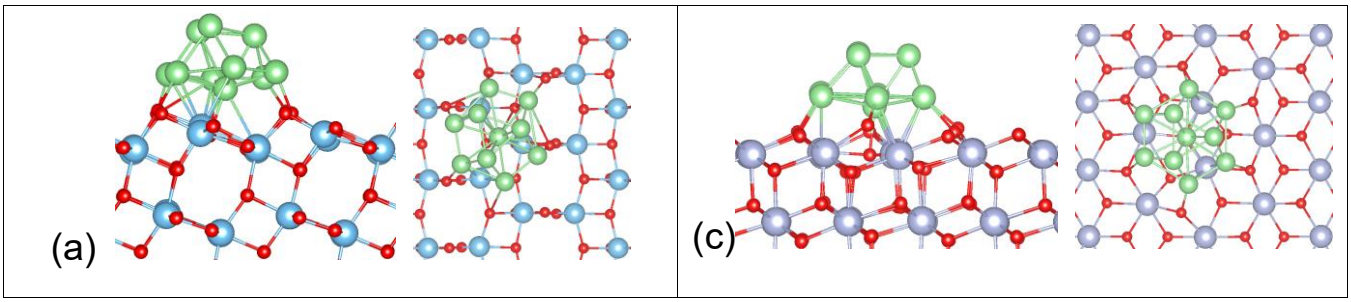

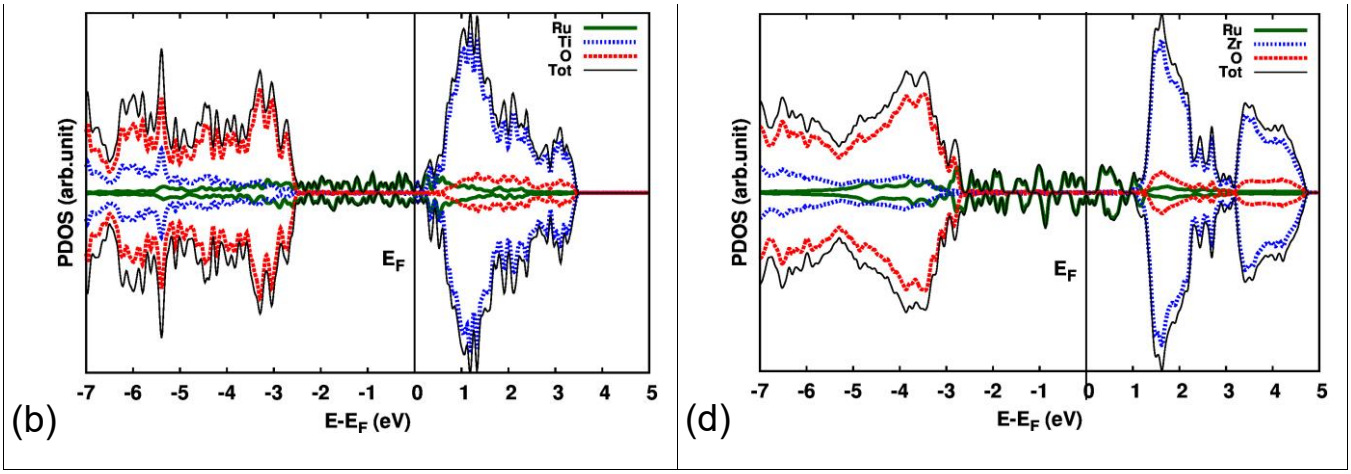

Figure 7. Left: Ru_{10} cluster adsorption on a-TiO_2(101); (a) Structures (side and top view); (b) projected DOS. Right: Ru_{10} cluster adsorption on t-ZrO_2(101); (c) Structures (side and top view); (d) projected DOS. The zero of energy corresponds to the Fermi level.

So far we have considered only structures of the Ru_{10} cluster where the original (7,3) layered structure is preserved also after adsorption on the surface. However, in some cases the original structure is completely lost after optimization. This is basically restricted to the a-TiO_2 (101) surface which exhibits a higher level of corrugation compared to the t-ZrO_2 (101) surface. In particular, there are three different types of O atoms (with different coordination) on a-TiO_2 (101) and the corrugation due to the surface structure is about 1.6 Å. Although the t-ZrO_2(101) surface also displays a zigzag profile, the corrugation is much smaller, 0.8 Å, and there is only one type of O site. The indentation in the anatase surface allows for more metal atoms to be accommodated into this depression. For instance, by adsorbing the Ru_{10} cluster with a reversed orientation, (3,7) instead of (7,3), one can fill with Ru atoms the valleys in the anatase surface. When the cluster is reoptimized, the shape changes completely and does not resemble anymore the initial structure (see Figure 8). The adsorption energy of this Ru_{10}(6,4) isomer is about 1 eV larger, in absolute value, than the corresponding case of the Ru_{10}(7,3) isomer, Table 3. This is different on zirconia where the Ru_{10}(3,7) cluster does not fit with the surface morphology and the resulting energy is higher than the Ru_{10}(7,3) case discussed above. The nature of the bonding of the more stable Ru_{10}(6,4) isomer on a-TiO_2 does not differ substantially from that described above for the less distorted Ru_{10}(7,3) cluster. Also in this case, in fact, there is no clear evidence of a direct reduction of the oxide support, Table 3. To sum up, the deformed Ru_{10} cluster only forms on TiO_2 (101) and not ZrO_2 (101) surfaces, but the bonding to the surface resembles that of the less distorted structure.

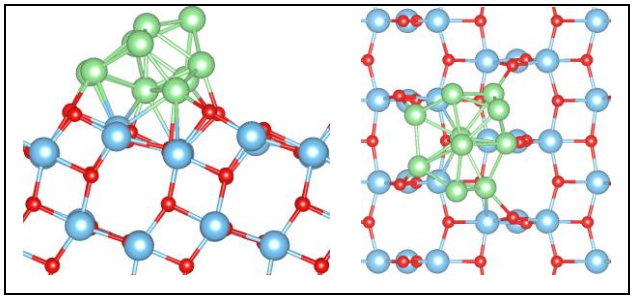

Figure 8. Side and top views of TiO_2/Ru_{10}(6,4) distorted cluster.

3.3.2 Ru_{10} on reduced a-TiO_{2-x} and t-ZrO_{2-x}

We consider now the adsorption of Ru_{10} on the reduced TiO_{2-x} and ZrO_{2-x} surfaces. Here the situation is considerably more complex since the vacancy can be created in various positions. For every vacancy the structure of Ru_{10} has been re-optimized. We restrict the discussion to some relevant cases.

We have explored several possible configurations by removing each of the O atoms directly bound to one of the Ru atoms of the cluster (vacancy at the metal/oxide interface); the central Ru atom of the bottom layer of Ru_{10} has been placed on top of O_{2c} and O_{3c} atoms, as for the stoichiometric surface. Among all of configurations, the most stable ones with the central Ru on O_{3c} and O_{2c} sites are considered. The adsorption mode with the O_{3c} site at the center (E_{ads} = -8.20 eV, Table 3 and Figure 9(a)) is preferred with respect to the O_{2c} case (E_{ads} = -7.20 eV), for the same reasons discussed for the non-defective surface, Table 3. The adsorption energy increases markedly, going from about 6 eV on the stoichiometric surface to more than 8 eV on the reduced one, Table 3. A similar effect has been found for Pt and Au clusters on the same surface.[61] The presence of the O vacancy below the cluster is essential for its stabilization. In fact, if the vacancy is far from the cluster the resulting Ru_{10}/TiO_{2-x} structure is about 1.4 less stable, Table 3. Focusing on the most stable configuration, the Bader charge of Ru_{10} is +0.5 |e|, i.e. 0.68 |e| smaller than on the regular surface, Table 3. Since the Ru_{10} structure and adsorption site are very similar, we can conclude that there is charge redistribution from the O vacancy towards Ru_{10} cluster which contributes to reinforce the bonding of the cluster to the surface.

When the O vacancy is in the sub-surface, Figure 9(b), the bonding of Ru_{10} to TiO_{2-x} is strongly reduced, E_{ads} = -5.95 eV, and becomes comparable to that of the same cluster on the stoichiometric surface, Table 3. From an electronic point of view we found that one of the two extra electrons associated to the vacancy is localized on one Ti atom, while the other becomes delocalized at the TiO_2/Ru interface (see the spin density plot in Figure S3). However, the structure and

adsorption energy of Ru_{10} adsorbed on stoichiometric TiO_2 or on reduced TiO_{2-x} with a vacancy in sub-surface regions (V_O4) are similar, suggesting that only when the defect centers migrate towards the surface they can have a direct effect on the interaction between Ru_{10} and TiO_2.

The next case to consider is that of Ru_{10} on ZrO_{2-x}, Figure 9(c) and (d). Also in this case we started by creating a surface O vacancy in two positions, under the metal cluster or far from it. Similarly to TiO_{2-x}/Ru_{10} the case where the removed O is away from Ru_{10} is about 0.9 eV less stable. Also for reduced zirconia the presence of the vacancy below the cluster, Figure 9(c), leads to a net increase in the adsorption energy which becomes -10.73 eV (it is -8.49 eV on the stoichiometric surface, Table 3). The Bader charge on Ru_{10} is -0.49 |e|, indicating an electron delocalization from the ZrO_{2-x} surface to the cluster.

When we create an O vacancy in the sub-surface (V_O4), Figure 9(d), the adsorption energy drops by 2.3 eV, in parallel with the results found for TiO_{2-x}/Ru_{10}, Table 3. Also in this case, in fact, the cluster structure, E_{ads} and Bader charge are very similar for ZrO_2/Ru_{10} and ZrO_{2-x}/Ru_{10} (sub-surface vacancy). Another sub-surface vacancy (V_O3) has been considered but this is meta-stable and tends to migrate to the surface and interact directly with the Ru_{10} cluster once this is adsorbed.

In summary, we found that on both TiO_2 and ZrO_2 surfaces the presence of an O vacancy on the surface results in a stronger adhesion and in a charge transfer from the surface to the cluster provided that the vacancy is in direct contact with the metal. On the contrary, if the O vacancy is far from the cluster (in sub-surface layers or on the surface but not in direct contact with the metal particle) the effect on the adsorption properties is minor and little differences are found between the stoichiometric and the reduced surfaces.

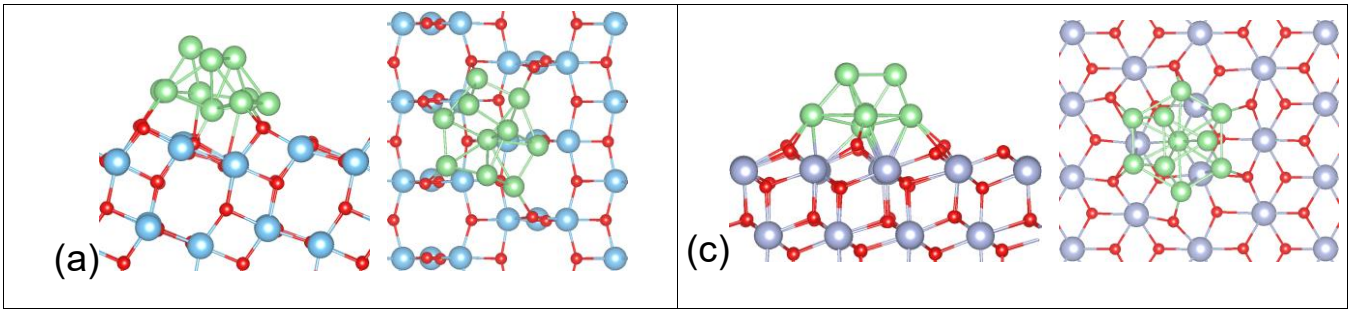

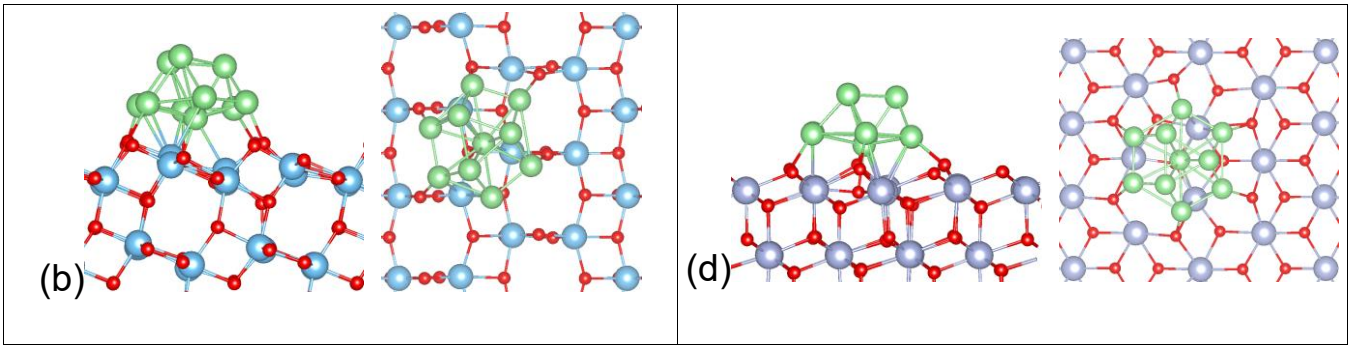

Figure 9 – Left: Ru_{10} adsorbed on reduced a-TiO_{2-x} (101) surface; (a) Side and top views, vacancy in the surface (V_O1); (b) Side and top views, vacancy in sub-surface (V_O4). Right: Ru_{10} adsorbed on reduced t-ZrO_{2-x} (101) surface; (c) Side and top views, vacancy in the surface (V_O1); (d) Side and top views, vacancy in sub-surface (V_O4).

3.4 Oxygen reverse spill-over on TiO_2/Ru_{10} and ZrO_2/Ru_{10}

We have mentioned in the introduction that one of the important aspects of the deposition of metal nanoparticles on the surface of titania and zirconia is that they can help the chemical reduction of the oxide support. This is relevant for the chemistry of the oxide catalyst in biomass conversion. Reduction of MO_2 can occur via at least three different mechanisms. The first one is the already mentioned direct transfer of electronic charge from the metal particle to the oxide support. This charge should be localized on specific ions giving rise to the formation of paramagnetic Ti^{3+} or Zr^{3+} species. A second possibility is that the metal nanoparticle helps the dissociation of H_2, the formation of H atoms that then bind to surface O ions as protons and transfer their valence electron to the oxide. This is an indirect process that requires the exposure to a specific reducing agent, hydrogen, and will be analyzed in a forthcoming study. The other chemical mechanism is the reduction of the oxide support by transfer of oxygen atoms from the oxide to the metal nanoparticle. This process is also known as oxygen reverse spillover, and removes oxygen from the surface leaving behind extra electrons that can occupy the empty d states of Ti or Zr ions. To study this latter process we have considered a model where an O atom directly below the Ru_{10} cluster is removed from the surface and bound to the cluster surface (various positions have been considered).

Based on the most stable configurations of TiO_{2-x}/Ru_{10} or ZrO_{2-x}/Ru_{10}, the O removed from the surface has been re-adsorbed on top of the (7,3) Ru_{10} structure (top adsorption) or on one of the lateral faces of the polyhedron (side or bridge adsorption, where side-n indicates the number of Ru atoms forming a lateral facet), Figure 10. In one case a stable structure was found where the O atom is incorporated below the Ru_{10} cluster, at the interface with the oxide (interface), Figure 10. In these models, TiO_{2-x}/Ru_{10}-O or ZrO_{2-x}/Ru_{10}-O, the total number of atoms in the supercell is exactly the

same for TiO_2/Ru_{10} or ZrO_2/Ru_{10} stoichiometric surfaces, and the respective total energies can be directly compared (see Table 4). A positive value of the spillover process, ΔE_{spill}, indicates an endothermic reaction. In this way an information on the thermodynamic stability of the initial (stoichiometric) and final (reduced) surfaces can be obtained. The barriers involved in the O displacement have not been investigated. Under experimental conditions the catalysts undergo a substantial thermal treatment that can provide the thermal energy required to overcome the barriers involved in the oxygen reverse spillover and reach thermodynamic equilibrium.

Table 4 - Oxygen reverse spillover, ΔE_{spill}, and Bader charges, q, of TiO_2/Ru_{10} and ZrO_2/Ru_{10}

	O ads. site	ΔE_{spill} (eV)	$q(Ru_{10})$ (|e|)
$Ti_{60}O_{120}/Ru_{10}$	-	0.00	1.18
$Ti_{60}O_{119}/Ru_{10}$-O [(a)]	Side-4	0.22	1.56
	Side-3	0.33	1.46
	Interface	0.27	1.16
	Top	0.54	1.28
$Ti_{60}O_{119}/Ru_{10}$-O [(b)]	Top	1.84	2.05
$Zr_{60}O_{120}/Ru_{10}$	-	0.00	0.28
$Zr_{60}O_{119}/Ru_{10}$-O [(a)]	Top	0.62	0.39
	Side-3	0.92	0.33
	Bridge	1.11	0.33
	Side-4	1.44	0.37

(a) The O vacancy has been created on the surface layer, below the Ru_{10} cluster

(b) The O vacancy has been created on the surface layer, far from the Ru_{10} cluster

All cases considered exhibit $\Delta E_{spill} > 0$, Table 4. However, the values are relatively small, indicating a small cost for the process on the (101) surface. More specifically, on TiO_2 adsorption of O on the one of Ru_{10}(7,3) results in very small cost of the spillover process, ΔE_{spill} = 0.22 eV and 0.33 eV, Figure 10 and Table 4. Adsorption at the interface has also a very small cost, 0.27 eV, while O adsorption on-top of Ru_{10} is less favorable, ΔE_{spill} = 0.54 eV, Table 4. In general, for anatase the removal of surface oxygen and its re-adsorption on a Ru nanoparticle is almost thermoneutral. Notice however that this is true only if the O vacancy is directly below the cluster or, in other words, if the removed oxygen comes from the metal/oxide interface. In fact, when we compute a case

where the O vacancy has been created far from the Ru_{10} cluster the entire process is energetically highly unfavourable and ΔE_{spill} is 1.84 eV, Table 4. Oxygen spillover will involve those O atoms that are in direct contact with the metal particle. The results for O spillover on TiO_2/Ru_{10} have been checked by considering also a totally distorted Ru_{10} cluster (results now shown for brevity) but the conclusions are the same: also in this case ΔE_{spill} = 0.25 eV indicates an almost thermoneutral process. In all cases the adsorption of O on Ru_{10} and the simultaneous formation of a V_O center below the cluster results in a positively charged Ru cluster, Table 4: the oxidizing effect of O adsorption is stronger than the reducing effect due to the delocalization of the electrons associated to the vacancy over the metal cluster.

On ZrO_2 the most stable structure with ΔE_{spill} = 0.62 eV corresponds to an O atom adsorbed on-top of the cluster, Figure 10 and Table 4. The adsorption on the lateral faces of the $Ru_{10}(7,3)$ cluster is clearly less favourable with ΔE_{spill} of the order of 1 eV or more, Table 4. The overall positive charge of Ru_{10} is much smaller than on TiO_2, Table 4. The reason is that here the charge delocalization from the surface O vacancy to the cluster is more effective than on TiO_2, see Table 3, compensating the oxidative effect of the adsorbed O atom.

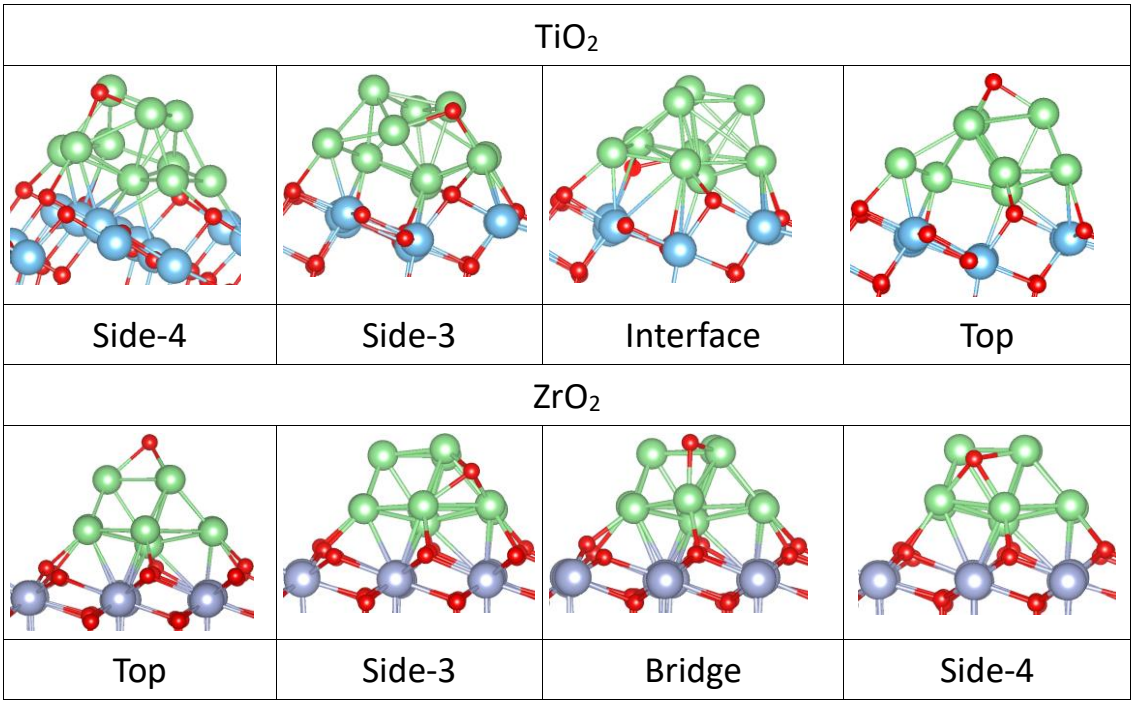

Figure 10 - Side view of the optimal structures of supported Ru_{10} clusters after O reverse spillover. Top: TiO_{2-x}/Ru_{10}-O; bottom: ZrO_{2-x}/Ru_{10}-O. Red: O; blue: Ti; violet: Zr; green: Ru.

The fact that the calculations consistently indicate a positive value for ΔE_{spill} should not lead to the conclusion that this mechanism is not relevant for the reduction of the supporting oxide. In fact, the calculations discussed so far refer to the flat, regular (101) surfaces of a-TiO_2 and t-ZrO_2. Things could be substantially different on surfaces exhibiting line defects like steps, or high number of undercoordinated atoms like on the surface of small nanoparticles. Various studies have shown that O removal from the surface of an oxide occurs preferentially in correspondence of morphological defects where atoms are low-coordinated. A recent study on O reverse spillover in the presence of Pt nanoparticles supported on CeO_2 has shown that while the process is endothermic on the regular (111) surface of CeO_2 it becomes thermodynamically favorable on ceria nanoparticles.[66] Our results show that on a-TiO_2 ΔE_{spill} is about 0.2 eV, a very small quantity. It is very likely that on a nanoparticle the same process will become exothermic. Different is the case of t-ZrO_2 where the lowest value of ΔE_{spill} is about 0.6 eV. Here the role of low-coordination is less easy to predict and requires further studies.

4. Conclusions

The adsorption properties of single Ru atoms and Ru_{10} clusters adsorbed on stoichiometric and reduced anatase TiO_2 and tetragonal ZrO_2 (101) surfaces have been considered based on a DFT+U approach. Ru/TiO_2 and Ru/ZrO_2 have been proposed as efficient catalysts for biomass conversion in biofuels, and in particular for the ketonization reaction, a key process in biofuel conversion. Experimental results indicate that the addition of a metal like Ru on the surface of the two oxides results in an increased catalytic activity,[13] in particular when the catalyst is subject to a pre-treatment in hydrogen. Metal deposition and reaction with hydrogen are all processes that lead to a reduction of the metal oxide. It has been suggested that these processes increase the number of exposed low-coordinated Ti and Zr ions on the surface of the catalyst, and that in particular reduced Ti^{3+} and Zr^{3+} ions may be the active sites in the ketonization process.[13] An unambiguous proof of the nature of the active sites is still missing, and this is also a motivation for this theoretical study.

We have investigated the effect of the addition of the Ru metal on the two oxide surfaces and performed a comparative study where the adsorption and electronic properties of the two systems are computed on an equal footing. Deposition of Ru isolated atom has been considered, i.e. the limit of ultra-dispersed supported metals, and a Ru_{10} three-dimensional cluster representative of Ru nanoparticles. Both stoichiometric and reduced surfaces have been considered, and the main objective is to verify the possible occurrence of a direct charge transfer from the Ru metal to the oxide surface, with consequent reduction of the oxide. This mechanism has been demonstrated for

other systems, like for instance Ag nanoparticles deposited on CeO_2.[67] The results, however, seem to rule out this possibility. For ZrO_2 we have no evidence of the formation of Zr^{3+} ions by deposition of Ru atoms or clusters. For TiO_2 the situation is a bit more complex as we have evidence of the formation of Ti^{3+} ions in some specific cases, but the total energy is always higher than that of the system with no charge transfer. This is consistent with the fact that TiO_2 is more reducible than ZrO_2. However, the general conclusion is that direct reduction of the TiO_2 or ZrO_2 supports does not occur by simple deposition of the Ru metal.

We have also considered an alternative process, the indirect reduction of the oxide by effect of an oxygen reverse spillover. In the presence of a metal nanoparticle O atoms diffuse from the surface of the oxide to the metal, leaving behind an oxygen vacancy with consequent reduction of the oxide. The thermodynamic cost to displace an O atom from the (101) surface of TiO_2 and ZrO_2 in the presence of a Ru nanoparticle has been estimated: it is very small, about 0.2 eV, on TiO_2, and moderate, about 0.6 eV, on ZrO_2. This means that on the regular (101) surface the process is endothermic. However, in general the formation of O vacancies on oxide surface is much lower on steps, edges, and other defects which are particularly abundant on the surface of oxide nanoparticles.[68,69] A reduction of the formation energy of the O vacancy by about 0.5 eV on a low-coordinated site would result in an exothermic O reverse spillover on TiO_2 and an almost thermoneutral process on ZrO_2. In this respect, the oxygen reverse spillover is a mechanism of potential interest for the reduction of the oxide surface. Of course, other processes like the exposure to hydrogen can be more efficient in terms of oxide reduction. Work is in progress in order to analyze the role of Ru/TiO_2 and Ru/ZrO_2 catalyst in hydrogen splitting and spill over.

Acknowledgments

This work has been supported by the European Community's Seventh Framework Programme FP7/2007-2013 under Grant Agreement n° 604307 (CASCATBEL) and by Italian MIUR through the FIRB Project RBAP115AYN “Oxides at the nanoscale: multifunctionality and applications”. The support of the COST Action CM1104 “Reducible oxide chemistry, structure and functions” is also gratefully acknowledged.

Supporting Information

Supporting Information is available free of charge via the Internet at http://pubs.acs.org

Table of content

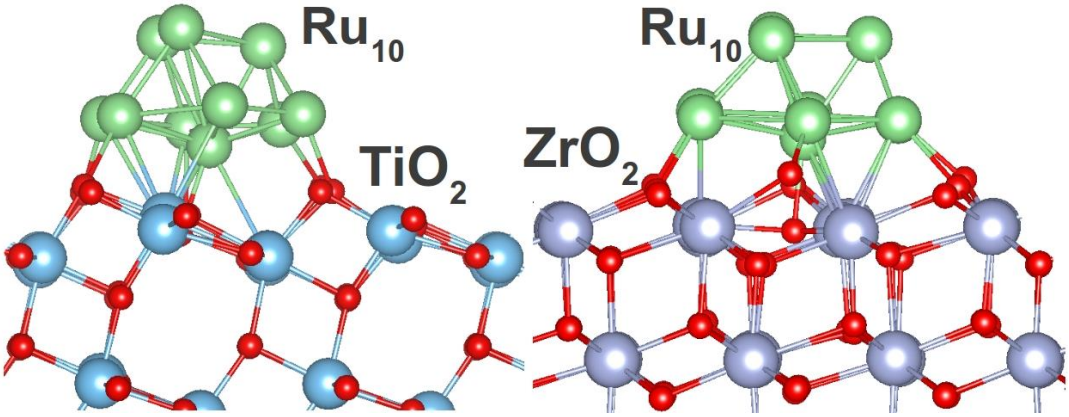

References

(1) Pacchioni, G. Electronic Interactions and Charge Transfers of Metal Atoms and Clusters on Oxide Surfaces. *Phys. Chem. Chem. Phys.* **2013**, *15*, 1737-1757.

(2) Libuda, J.; Freund, H. J. Molecular Beam Experiments on Model Catalysts, *Surf. Sci. Rep.*, **2005**, *57*, 157–298

(3) Somorjai, G. A.; Park, J. Y. Molecular Surface Chemistry by Metal Single Crystals and Nanoparticles from Vacuum to High Pressure, *Chem. Soc. Rev.*, **2008**, *37*, 2155–2162

(4) Bell, A. T. The Impact of Nanoscience on Heterogeneous Catalysis, *Science* **2003**, *299*, 1688-1691.

(5) Barteau, M. A. Organic Reactions at Well-Defined Oxide Surfaces. *Chem. Rev.* **1996**, *96*, 1413-1430.

(6) Shen, W. Q.; Tompsett, G. A.; Xing, R.; Conner, W. C.; Huber, G. W. Vapor Phase Butanal Self-Condensation over Unsupported and Supported Alkaline Earth Metal Oxides. *J. Catal.* **2012**, *286*, 248-259.

(7) Faba, L.; Díaz, E.; Ordóñez, S. One-Pot Aldol Condensation and Hydrodeoxygenation of Biomass-Derived Carbonyl Compounds for Biodiesel Synthesis. *ChemSusChem* **2014**, *7*, 2816-2820.

(8) Kikhtyanin, O.; Kubička, D.; Čejka, J. Toward Understanding of the Role of Lewis Acidity in Aldol Condensation of Acetone and Furfural Using MOF and Zeolite Catalysts. *Catal. Today* **2014**, DOI:http://dx.doi.org/10.1016/j.cattod.2014.08.016.

(9) Pham, T. N.; Sooknoi, T.; Crossley, S. P.; Resasco, D. E. Ketonization of Carboxylic Acids: Mechanisms, Catalysts, and Implications for Biomass Conversion. *ACS Catal.* **2013**, *3*, 2456-2473.

(10) Rajadurai, S., Pathways for Carboxylic-Acid Decomposition on Transition-Metal Oxides. *Catal. Rev.-Sci. Eng.* **1994**, *36*, 385-403.

(11) Pacchioni, G. Ketonization of Carboxylic Acids in Biomass Conversion over TiO_2 and ZrO_2 Surfaces: A DFT Perspective. *ACS Catal.* **2014**, *4*, 2874-2888.

(12) Pham, T. N.; Shi, D. C.; Resasco, D. E. Kinetics and Mechanism of Ketonization of Acetic Acid on Ru/TiO_2 Catalyst. *Top. Catal.* **2014**, *57*, 706-714.

(13) Pham, T. N.; Shi, D. C.; Resasco, D. E. Reaction Kinetics and Mechanism of Ketonization of Aliphatic Carboxylic Acids with Different Carbon Chain Lengths over Ru/TiO_2 Catalyst. *J. Catal.* **2014**, *314*, 149-158.

(14) Di Valentin, C.; Pacchioni, G.; Selloni, A. Reduced and N-Type Doped TiO_2: Nature of Ti^{3+} Species. *J. Phys. Chem. C* **2009**, *113*, 20543-20552.

(15) Gionco, C.; Paganini, M. C.; Giamello, E.; Burgess, R.; Di Valentin, C.; Pacchioni, G. Paramagnetic Defects in Polycrystalline Zirconia: an EPR and DFT Study. *Chem. Mater.* **2013**, 25, 2243−2253.

(16) Ghosh, T. B.; Dhabal, S.; Datta, A. K. On Crystallite Size Dependence of Phase Stability of Nanocrystalline TiO_2. *J. Appl. Phys.* **2003**, *94*, 4577-4582.

(17) Smith, S. J.; Stevens, R.; Liu, S. F.; Li, G. S.; Navrotsky, A.; Boerio-Goates, J.; Woodfield, B. F. Heat Capacities and Thermodynamic Functions of TiO_2 Anatase and Rutile: Analysis of Phase Stability. *Am. Mineral.* **2009**, *94*, 236-243.

(18) Hanaor, D. A. H.; Sorrell, C. C. Review of the Anatase to Rutile Phase Transformation. *J. Mater. Sci.* **2011**, *46*, 855-874.

(19) Augustynski, J. The Role of the Surface Intermediates in the Photoelectrochemical Behavior of Anatase and Rutile TiO_2. *Electrochim. Acta* **1993**, *38*, 43-46.

(20) Linsebigler, A. L.; Lu, G. Q.; Yates, J. T. Photocatalysis on TiO_2 Surfaces - Principles, Mechanisms, and Selected Results. *Chem. Rev.* **1995**, *95*, 735-758.

(21) Hadjiivanov, K. I.; Klissurski, D. G. Surface Chemistry of Titania (Anatase) and Titania-Supported Catalysts. *Chem. Soc. Rev.* **1996**, *25*, 61-69.

(22) Kavan, L.; Gratzel, M.; Gilbert, S. E.; Klemenz, C.; Scheel, H. J. Electrochemical and Photoelectrochemical Investigation of Single-Crystal Anatase. *J. Am. Chem. Soc.* **1996**, *118*, 6716-6723.

(23) Diebold, U.; Ruzycki, N.; Herman, G. S.; Selloni, A. One Step Towards Bridging the Materials Gap: Surface Studies of TiO_2 Anatase. *Catal. Today* **2003**, *85*, 93-100.

(24) Leger, J. M.; Tomaszewski, P. E.; Atouf, A.; Pereira, A. S. Pressure-Induced Structural Phase-Transitions in Zirconia under High-Pressure. *Phys. Rev. B* **1993**, *47*, 14075-14083.

(25) Kisi, E. H.; Howard, C. J. Crystal Structures of Zirconia Phases and Their Inter-Relation. *Key Eng. Mat.* **1998**, *153-154*, 1-39.
(26) Dash, L. K.; Vast, N.; Baranek, P.; Cheynet, M. C.; Reining, L. Electronic structure and electron energy-loss spectroscopy of ZrO_2 zirconia. *Phys. Rev. B* **2004**, *70*, 245116.
(27) Shukla, S.; Seal, S. Mechanisms of Room Temperature Metastable Tetragonal Phase Stabilisation in Zirconia. *Int. Mater. Rev.* **2005**, *50*, 45-64.
(28) Dwivedi, A.; Cormack, A. N. A Computer-Simulation Study of the Defect Structure of Calcia-Stabilized Zirconia. *Philos. Mag.* **1990**, *61*, 1-22.
(29) Kharton, V. V.; Marques, F. M. B.; Atkinson, A. Transport Properties of Solid Oxide Electrolyte Ceramics: A Brief Review. *Solid State Ion.* **2004**, *174*, 135-149.
(30) Guo X. Low Temperature Stability of Cubic Zirconia. *Phys. Status Solidi A* **2000**, *177*, 191-201.
(31) Stefanovich, E. V.; Shluger, A. L.; Catlow C. R. A. Theoretical Study of the Stabilization of Cubic-Phase ZrO_2 by Impurities. *Phys. Rev. B* **1994**, *49*, 11560-11571.
(32) Hofmann, A.; Clark, S.J.; Oppel, M.; Hahndorf, I. Hydrogen Adsorption on the Tetragonal ZrO_2 Surface: a Theoretical Study of an Important Catalytic Reactant. *Phys. Chem. Chem. Phys.* **2002**, *4*, 3500-3508.
(33) Kresse, G.; Furthmüller, J. Efficiency of Ab-Initio Total Energy Calculations for Metals and Semiconductors Using a Plane-Wave Basis Set. *J. Comput. Mater. Sci*. **1996**, *6*, 15-50.
(34) Blöchl, P. E. Projector Augmented-Wave Method. *Phys. Rev. B* **1994**, *50*, 17953-17979.
(35) Kresse, G.; Joubert, J. From Ultrasoft Pseudopotentials to the Projector Augmented-Wave Method. *Phys. Rev. B* **1999**, *59*, 1758-1775.
(36) Perdew, J. P.; Burke, K.; Ernzerhof, M. Generalized Gradient Approximation Made Simple. *Phys. Rev. Lett.* **1996**, *77*, 3865-3868.
(37) Anisimov, V. I.; Zaanen, J.; Andersen, O. K. Band Theory and Mott Insulators - Hubbard-U Instead of Stoner-I. *Phys. Rev. B* **1991**, *44*, 943-954.
(38) Dudarev, S. L.; Botton, G. A.; Savrasov, S. Y.; Humphreys, C. J.; Sutton, A. P. Electron-Energy-Loss Spectra and the Structural Stability of Nickel Oxide: An LSDA+U Study. *Phys. Rev. B* **1998**, *57*, 1505-1509.
(39) Dagotto, E. Correlated Electrons in High-temperature Superconductors *Rev. Mod. Phys.* **1994**, *66*, 763-840.
(40) Moreira, I. de P. R.; Illas, F.; Martin, R.L. Effect of Fock Exchange on the Electronic Structure and Magnetic Coupling in NiO *Phys. Rev. B* **2002**, *65*, 155102.
(41) Rivero, P.; Moreira, I. de P.R.; Illas, F. Electronic Structure of Single-layered Undoped Cuprates from Hybrid Density Functional Theory *Phys. Rev. B*, **2010**, 81, 205123.
(42) Tosoni, S.; Lamiel-Garcia, O.; Fernandez Hevia, D.; Do a, J. M.; Illas, F. Electronic Structure of F-Doped Bulk Rutile, Anatase, and Brookite Polymorphs of TiO_2. *J. Phys. Chem. C* **2012**, *116*, 12738-12746.
(43) Ortega, Y.; Lamiel-Garcia, O.; Fernandez Hevia, D.; Tosoni, S.; Oviedo, J.; San-Miguel, M. A.; Illas, F. Theoretical Study of the Fluorine Doped Anatase Surfaces. *Surf. Sci.* **2013**, *618*, 154-158.
(44) Syzgantseva, O. A.; Calatayud, M.; Minot, C. Revealing the Surface Reactivity of Zirconia by Periodic DFT Calculations. *J. Phys. Chem. C* **2012**, *116*, 6636-6644.
(45) Christensen, A.; Carter, E. A. First-Principles Study of the Surfaces of Zirconia. *Phys. Rev. B* **1998**, *58*, 8050-8064.
(46) Haase, F.; Sauer, J. The Surface Structure of Sulfated Zirconia: Periodic Ab Initio Study of Sulfuric Acid Adsorbed on ZrO_2(101) and ZrO_2(001) *J. Am. Chem. Soc.* **1998**, *120*, 13503-13512.
(47) Eichler, A.; Kresse, G. First-Principles Calculations for the Surface Termination of Pure and Yttria-Doped Zirconia Surfaces. *Phys. Rev. B* **2004**, *69*, 045402.
(48) Ganduglia-Pirovano, M.V.; Hofmann, A.; Sauer, J. Oxygen Vacancies in Transition Metal and Rare Earth Oxides: Current State of Understanding and Remaining Challenges. *Surf. Sci. Rep.* **2007**, *62*, 219-270.
(49) Bader R. F. W. A Quantum Theory of Molecular Structure and its Applications. *Chem. Rev.* **1991**, *91*, 893-928.

(50) Bredow, T.; Giordano, L.; Cinquini, F.; Pacchioni, G. Electronic Properties of Rutile TiO_2 Ultrathin Films: Odd-Even Oscillations with the Number of Layers. *Phys. Rev. B* **2004**, *70*, 035419.
(51) Hu, Z. P.; Metiu, H. Choice of U for DFT Plus U Calculations for Titanium Oxides. *J. Phys. Chem. C* **2011**, *115*, 5841-5845.
(52) McComb, D.W. Bonding and Electronic Structure in Zirconia Pseudopolymorphs Investigated by Electron Energy-loss Spectroscopy *Phys. Rev. B* **1996**, *54*, 7094-7102.
(53) French, R. H.; Glass, S. J.; Ohuchi, F. S.; Xu, Y. N.; Ching, W. Y. Experimental and Theoretical Determination of the Electronic-Structure and Optical-Properties of 3 Phases of ZrO_2 *Phys. Rev. B* **1994**, *49*, 5133-5141.
(54) Scanlon, D. O.; Dunnill, C. W.; Buckeridge, J.; Shevlin, S. A.; Logsdail, A. J.; Woodley, S. M.; Catlow, C. R. A.; Powell, M. J.; Palgrave, R. G.; Parkin, I. P.; et al. Band Alignment of Rutile and Anatase TiO_2. *Nat. Mater.* **2013**, *12*, 798-801.
(55) Cheng, H. Z.; Selloni, A. Energetics and Diffusion of Intrinsic Surface and Subsurface Defects on Anatase TiO2 (101). *J. Chem. Phys.* **2009**, *131*, 054703.
(56) Cheng, H. Z.; Selloni, A. Surface and Subsurface Oxygen Vacancies in Anatase TiO_2 and Differences with Rutile. *Phys. Rev. B* **2009**, *79*, 092101.
(57) He, Y. B.; Dulub, O.; Cheng, H. Z.; Selloni, A.; Diebold, U. Evidence for the Predominance of Subsurface Defects on Reduced Anatase TiO_2(101). *Phys. Rev. Lett.* **2009**, *102*, 106105.
(58) Herzing, A. A.; Kiely, C. J.; Carley, A. F.; Landon, P.; Hutchings, G. J. Identification of Active Gold Nanoclusters on Iron Oxide Supports for Co Oxidation. *Science* **2008**, *321*, 1331-1335.
(59) Yang, X.-F.; Wang, A.; Qiao, B.; Li, J.; Liu, J.; Zhang, T. Single-Atom Catalysts: A New Frontier in Heterogeneous Catalysis. *Accounts Chem. Res.* **2013**, *46*, 1740-1748.
(60) Lin, J.; Wang, A.; Qiao, B.; Liu, X.; Yang, X.; Wang, X.; Liang, J.; Li, J.; Liu, J.; Zhang, T. Remarkable Performance of Ir_1/FeO_x Single-Atom Catalyst in Water Gas Shift Reaction. *J. Am. Chem. Soc.* **2013**, *135*, 15314-15317.
(61) Gong, X.-Q.; Selloni, A.; Dulub, O.; Jacobson, P.; Diebold, U. Small Au and Pt Clusters at the Anatase TiO_2(101) Surface: Behavior at Terraces, Steps, and Surface Oxygen Vacancies. *J. Am. Chem. Soc.* **2008**, *130*, 370-381.
(62) Zhang, S.-T.; Li, C.-M.; Yan, H.; Wei, M.; Evans, D. G.; Duan, X. Density Functional Theory Study on the Metal-Support Interaction between Ru Cluster and Anatase TiO_2 (101) Surface. *J. Phys. Chem. C* **2014**, *118*, 3514-3522.
(63) Grau-Crespo, R.; Cruz Hernández, N.; Sanz, J.F.; de Leeuw, N. H. Theoretical Investigation of the Deposition of Cu, Ag, and Au Atoms on the ZrO_2(111) Surface *J. Phys. Chem. C* **2007**, *111*, 10448-10454.
(64) Vilhelmsen, L.B.; Hammer, B. A Genetic Algorithm for First Principles Global Structure Optimization of Supported Nano Structures *J. Chem. Phys.* **2014**, *141*, 044711.
(65) Li, C.-M.; Zhang, S. T.; Zhang, B. S.; Su, D. S.; He, S.; Zhao, Y. F.; Liu, J.; Wang, F.; Wei, M.; Evans, D. G.; et al. Photohole-Oxidation-Assisted Anchoring of Ultra-small Ru Clusters onto TiO_2 with Excellent Catalytic Activity and Stability. *J. Mater. Chem. A* **2013**, *1*, 2461−2467.
(66) Vayssilov, G. N.; Lykhach, Y.; Migani, A.; Staudt, T.; Petrova, G. P.; Tsud, N.; Skála, T.; Bruix, A.; Illas, F.; Prince, K. C.; et al. Support Nanostructure Boosts Oxygen Transfer to Catalytically Active Platinum Nanoparticles. *Nat. Mater.* **2011**, *10*, 310-315.
(67) Luches, P.; Pagliuca, F.; Valeri, S.; Illas, F.; Preda, G.; Pacchioni, G. Nature of Ag Islands and Nanoparticles on the CeO_2 (111) Surface. *J. Phys. Chem. C* **2012**, *116*, 1122-1132.
(68) Pacchioni, G.; Pescarmona, P. Structure and Stability of Oxygen Vacancies on Sub-Surface, Terraces, and Low-Coordinated Surface Sites of Mgo: An Ab Initio Study. *Surf. Sci.* **1998**, *412-13*, 657-671.
(69) Pacchioni, G.; Freund, H. Electron Transfer at Oxide Surfaces. The MgO Paradigm: From Defects to Ultrathin Films. *Chem. Rev.* **2013**, *113*, 4035-4072.